In vivo nerve identification in head and neck surgery using diffuse reflectance spectroscopy

Langhout, Gerrit C.; Kuhlmann, Koert F.D.; Schreuder, Pim; Bydlon, Torre; Smeele, Ludi E.; van den Brekel, Michiel W.M.; Sterenborg, Henricus J.C.M.; Hendriks, Benno H.W.; Ruers, Theo J.M.

DOI
10.1002/lio2.174

Publication date
2018

Document Version
Final published version

Published in
Laryngoscope investigative otolaryngology

Citation (APA)
Langhout, G. C., Kuhlmann, K. F. D., Schreuder, P., Bydlon, T., Smeele, L. E., van den Brekel, M. W. M., Sterenborg, H. J. C. M., Hendriks, B. H. W., & Ruers, T. J. M. (2018). In vivo nerve identification in head and neck surgery using diffuse reflectance spectroscopy. *Laryngoscope investigative otolaryngology*, *3*(5), 349-355. https://doi.org/10.1002/lio2.174

Laryngoscope Investigative Otolaryngology

In Vivo Nerve Identification in Head and Neck Surgery Using Diffuse Reflectance Spectroscopy

Gerrit C. Langhout, MD; Koert F.D. Kuhlmann, MD, PhD; Pim Schreuder, MD, PhD; Torre Bydlon, PhD; Ludi E. Smeele, MD, PhD; Michiel W.M. van den Brekel, MD, PhD; Henricus J.C.M. Sterenborg, PhD; Benno H.W. Hendriks, PhD; Theo J.M. Ruers, MD, PhD

Background: Careful identification of nerves during head and neck surgery is essential to prevent nerve damage. Currently, nerves are identified based on anatomy and appearance, optionally combined with electromyography (EMG). In challenging cases, nerve damage is reported in up to 50%. Recently, optical techniques, like diffuse reflectance spectroscopy (DRS) and fluorescence spectroscopy (FS) show potential to improve nerve identification.

Methods: 212 intra-operative DRS/FS measurements were performed. Small nerve branches (1–3 mm), on near-nerve adipose tissue, muscle and subcutaneous fat were measured during 11 surgical procedures. Tissue identification was based on quantified concentrations of optical absorbers and scattering parameters.

Results: Clinically comprehensive parameters showed significant differences (<0.05) between the tissues. Classification using k-Nearest Neighbor resulted in 100% sensitivity and a specificity of 83% (accuracy 91%), for the identification of nerve against surrounding tissues.

Conclusions: DRS/FS is a potentially useful intraoperative tool for identification of nerves from adjacent tissues.

Key Words: Head and heck, surgery, peripheral nerves, diffuse reflectance spectroscopy, DRS.

Level of Evidence: Observational proof of principle study.

A Special Visual Abstract has been developed for this paper. (Visual Abstract 1)

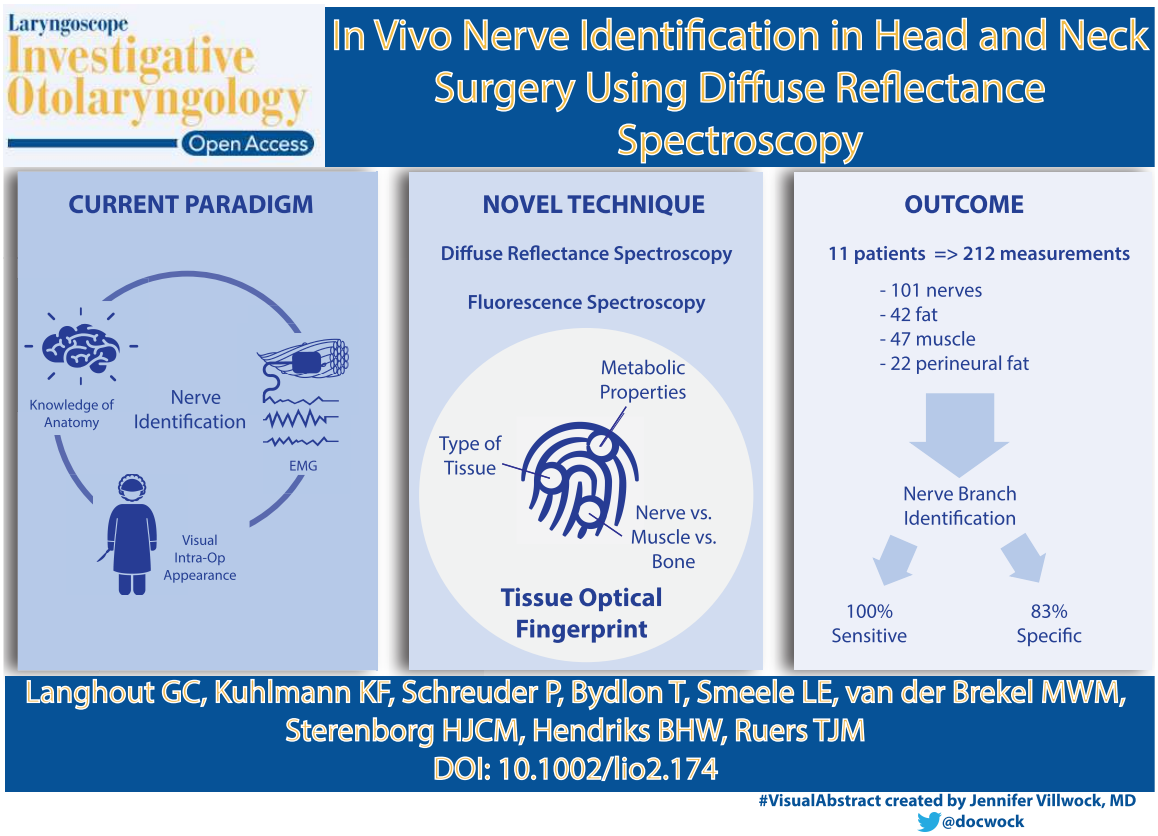

INTRODUCTION

The identification and preservation of peripheral nerves is essential during head and neck surgery as well as other surgery. Accidental transection or injury can cause severe morbidity including pain, numbness, weakness or paralysis. The incidence of damage to peripheral nerve branches varies. Nerve damage (including temporary neuropraxia) may be up to 50% for peripheral branches of the facial nerve during parotid surgery.[1] Conventionally, nerves are identified based on their anatomical position and visual appearance. In addition, electromyography (EMG) combined with local stimulation may be used to identify nerve tissue. This technique, however, requires an intact nerve pathway and functioning muscle. Furthermore, EMG identifies only motor pathways, not sensory fibers such as the first two divisions of the trigeminal nerve or the cochleovestibular nerve.[2] In addition, neuromuscular transmissions, and therefore muscle activity, may be hampered by nerve compression, tumor invasion, trauma, or medication. A systematical review indicates a successful localization of peripheral nerves using nerve stimulation in 80% (failure in 20%) of the cases. The review includes 32 RTCs concerning ultrasound and peripheral nerve stimulation guidance for nerve blocks in both upper and lower limbs.[3]

In the present paper we describe the use of diffuse reflectance spectroscopy (DRS) combined with fluorescence spectroscopy (FS) for the identification of small peripheral nerves. This optical technique was earlier used to identify various malignancies in breast,[4–6] liver,[7,8] colon,[9,10] cervix,[11] and lung.[12,13] In DRS, the tissue is illuminated with broadband white light. Within the tissue the light will be partly absorbed and will undergo scattering, depending on the specific tissue properties of the tissue. These interactions result in a tissue-specific "optical fingerprint" as measured by diffuse reflectance spectroscopy. Additionally, DRS measurements may be accompanied by fluorescence spectroscopy which is able to detect specific intrinsic fluorophores within the tissue such as collagen and elastin as well as tissue metabolism by parameters such as NADH and FAD.

Several studies have demonstrated the potential of optical spectroscopy for identification of peripheral nerves. These studies, however, are often targeting large nerves, as relevant for regional anesthesia.[14–17] Results obtained in swine and humans showed an excellent differentiation (area under the ROC curve, receiver operating characteristic curve, of 0.98) between muscle, fascia, and the targeted region for regional anesthesia. In another study by Schols et al., DRS was used to differentiate between nerve and adipose tissue, showing an accuracy between 67% and 100% depending on the validation method and sensor type.[16] Comparable results were described by Hendriks et al., who was able to identify nerve tissue using DRS with a sensitivity and specificity of around 90% in a post-mortem study in humans.[17]

The aim of the current in vivo study is to evaluate whether a combination of diffuse reflectance spectroscopy and fluorescence spectroscopy is able to identify small nerve branches during operative procedures in head and neck surgery. To this end we compared both the measured spectra as well as the derived optical properties from these spectra to differentiate between nerve tissue, subcutaneous fat, skeletal muscle, and nerve-surrounding adipose tissue during head and neck surgery.

The novelty of this study lies in the combination of in vivo human measurements under surgical conditions, the usage of clinical comprehensive parameters for both DRS and FS, and the inclusion of different types of surrounding tissues for the identification of small peripheral nerves.

MATERIALS AND METHODS

This study was performed at The Netherlands Cancer Institute–Antoni van Leeuwenhoek under approval of the protocol and ethics review board (NL40893.031.12). Written informed consent was obtained from all subjects. Patients undergoing total parotidectomy, mandibulectomy and partial glossectomy combined with block dissection of cervical lymph nodes and cervical lymph node dissection alone were randomly selected. The surgeries were performed using standard surgical instruments (sharp dissection by scalpel, blunt dissection by scissors/forceps, and coagulation by electrocoagulation). In all patients, the indication for surgery was a malignant tumor in the head and neck region.

Instrumentation

DRS and FS spectra were acquired using a spectroscopy system, described earlier.[6] For this study, a measurement probe containing four optical fibers with 200 μm core diameter (Invivo Germany, Schwerin, Germany) was used that delivered broad spectrum light from a tungsten-halogen source (AvaLight HAL-S-IND 20W, Avantes, Apeldoorn, the Netherlands) to the tissue. Two spectrometers (DU420A-BRDD and DU492A-1.7, Andor Technology, Belfast, Northern Ireland) covering the visible- and near-infrared range measured the diffusely reflected light from 400 to 1600 nm. Both sensors are cooled to -40 degrees Celsius during operation. A long-pass filter (BLP01-405R, Semrock, Rochester, New York, USA) prevented the recording of scattered laser (excitation) light during fluorescence excitation. Separate fibers with an intermediate distance of 0.8 mm were used as emitting and collecting fibers. A fiber splitter was used to distribute the collected light to the two spectrometers. FS

From the Department of Surgery (G.C.L., K.F.D.K., H.J.C.M.S., T.J.M.R.), the Department of Head and Neck Oncology and Surgery (P.S., L.E.S., M.W.M.B.), The Netherlands Cancer Institute–Antoni van Leeuwenhoek, Amsterdam, the Netherlands; In-Body Systems Department (T.B., B.H.W.H.), Philips Research, Eindhoven, the Netherlands; the Department of head and neck and Physics (L.E.S., H.J.C.M.S.), Academic Medical Center, Amsterdam, the Netherlands the Department of Biomechanical Engineering (B.H.W.H.), Delft University of Technology, Delft, the Netherlands the Nanobiophysics Group, (T.J.M.R.), MIRA Institute, University of Twente, Enschede, the Netherlands

Editor's Note: This Manuscript was accepted for publication 30 April 2018.

For this study, the Netherlands Cancer Institute received an unrestricted grant from Philips Research. This research was further supported by a grant of the KWF-Alpe d'HuZes (NKI 2014-6596).

Send correspondence to G.C. Langhout. Plesmanlaan 121, 1066 CX Amsterdam, the Netherlands. Email: N.langhout@nki.nl.

DOI: 10.1002/lio2.174

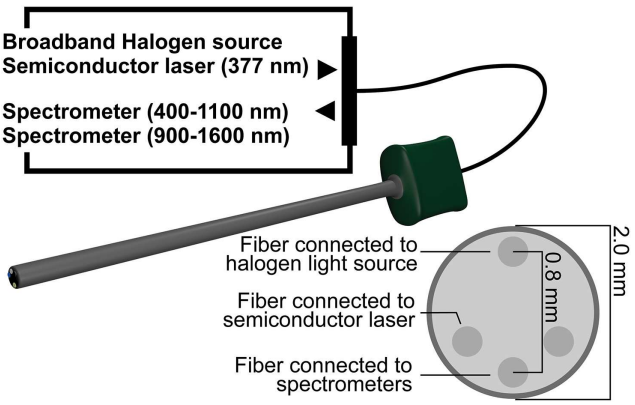

Fig. 1. Representation of the setup. The tissue is illuminated with broadband white light and laser light through separate optical fibers. A fiber splitter connected to the collecting fiber distributes the reflected light over the spectrometers. One fiber is not used and covered at the connector.

measurements were performed milliseconds after the DRS acquisition, creating the aspect of a single measurement. For FS, the system was equipped with a semiconductor laser (377 nm, 0.4 mW, NDU113E, Nichia, Tokyo, Japan) to induce auto fluorescence. A schematic representation of the setup is shown in Figure 1. The details of the setup and the corresponding calibration procedures are extensively discussed by Nachabe et al.[18] The measurement setup is controlled by custom made LabView software (National Instruments, Austin, Texas, USA).

Optical Measurements

Optical measurements were performed after surgical exposure of the nerve. Routine hemostasis was pursued and optical measurements were performed by placing the probe directly on the tissue of interest. During the measurement, the surgical lights were dimmed to minimize the influence of environmental light. A combined measurement (DRS and FS) was recorded within one second.

Four tissue groups were measured including subcutaneous fat, skeletal muscle, near-nerve adipose tissue, and nerve. Near-nerve adipose tissue is the adipose tissue surrounding several nerve branches. The nerve branch itself is not part of the tissue type. Depending on the availability of exposed nerves, measurements were performed on the greater auricular nerve (branch of the cervical plexus composed of branches of spinal nerves C2 and C3), the spinal accessory nerve (CN XI), or the facial nerve (CN VII). The diameter of the nerve branches varied from 1 to 3 mm. All optical measurements were acquired on unique locations.

Spectral Analysis

A widely accepted mathematical model first described by Farrell et al. was used to translate the measured spectra into absorption and scattering coefficients.[19] The absorption coefficients represent the concentration of physiologically relevant absorbers in the tissue, such as hemoglobin, water and fat (lipids), as well as functional parameters like oxygen saturation.[20] The main scattering parameters are the reduced scattering coefficient (at 800 nm), the reduced scattering slope of the Mie scattering (Mie-scattering slope), and the Mie-to-total scattering fraction.[21] The Mie-scattering slope is related to the average particle size.[22] The implementation of this model to analyze diffuse reflectance spectra over a wavelength of 400 to 1600 nm measured with the current setup is described by Nachabé.[23] Application of this model is described in various pre-clinical and clinical models.[7,9,24–26] Spectra highly contaminated by blood (>25%) were excluded from analysis. For FS, autofluorescence was calculated by correcting the measured fluorescence spectra for absorption and scattering using a method described earlier.[27,28] The model was implemented according to Müller[27] based on a modified photomigration model.[28] The corrected spectra were fitted using the intrinsic fluorescence spectra (excitation at 377 nm) of collagen, elastin, NADH, and FAD as a priori knowledge. A Mann–Whitney U test was used to compare the measurements of surrounding tissue with on-nerve. A P value < .05 indicates a significant difference between the two groups.

Tissue Classification and Statistics

The classification algorithm and statistics were conducted in Matlab (Matworks Inc., Natrick, Massachusetts, USA). Tissue was classified according to the k-Nearest Neighbors (knn) principle with k = 3. In this test, tissue was assigned to the class of the majority of the three nearest measurements from a training set. The training and validation sets were composed using leave-one-out cross-validation, ie, subsequently taking out the spectra of one patient as the validation set and using the remaining spectra for training. Input for the algorithm were the parameters derived from the DRS and FS spectra: water, fat, blood, β-carotene, methemoglobin and collagen concentration, fat fraction (fat/[water +fat]), hemoglobin oxygen saturation, mie scatter slope, scattering at 800 nm, total fluorescence signal, and FAD concentration. Parameters were normalized to a mean value of 0 with a standard deviation of 1, to give parameters an equal weight. This classification was repeated after omitting the parameters derived from fluorescence to determine the contribution of fluorescence to the classification.

The estimation of clinical comprehensive parameters from the spectra is a form of feature reduction. This approach gives insight in the composition of the tissue and helps to understand the measurement analysis, since results can be directly linked to well-known clinical tissue characteristics. However spectral information might be lost during the feature reduction. For this reason we also used principal component analysis (PCA) with 20 components as an alternative method of feature reduction.

The result of these classifications is an estimation of the sensitivity, specificity and Matthews correlation coefficient (MCC). This coefficient is used in machine learning as a measure of quality of classifications.[29] A MCC of + 1 represents a perfect prediction; -1 indicates total disagreement between prediction and observation.

RESULTS

Patient Characteristics

Eleven patients were included (age 63 ± 9 years): six males and five females. None of the patients had received neoadjuvant radio/chemo therapy. Five of the surgical procedures were mandibulectomy and partial glossectomy including block dissection of cervical lymph nodes, four patients underwent a cervical lymph node dissection alone, and in two patients a parotidectomy.

Tissue Spectra

Two hundred twelve optical measurements were performed: 42 on subcutaneous fat, 47 on muscle, 22 on near-nerve adipose tissue, and 101 on the nerve directly.

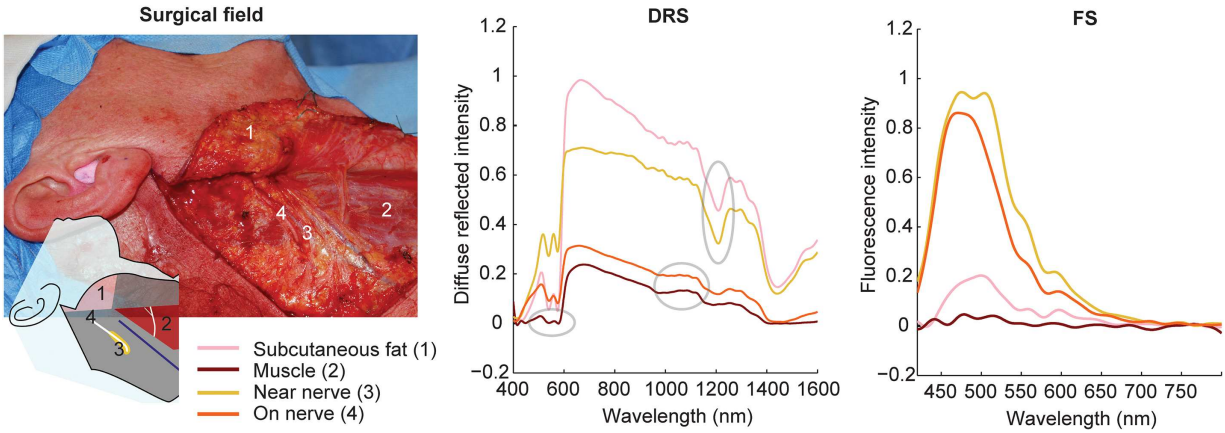

Fig. 2. DRS and FS measured spectra with the corresponding measurement locations. The schematic inlay indicates the locations marked by numbers related to the legend of the spectra. In the DRS spectrum, spectral characteristics of hemoglobin (left), water (middle) and fat (right) are depicted with a gray ellipse. The fluorescence spectra are not normalized nor corrected for absorption, to display the differences in fluorescence intensity.
DRS = diffuse reflectance spectroscopy.

An example of measured DRS and FS spectra is visualized in Figure 2. In the DRS spectra, the first segment (400–650 nm) is dominated by optical absorption of hemoglobin, myoglobin, and, to a lesser extent, beta-carotene. In this spectral region, muscle shows little intensity, indicating relatively high amounts of hemoglobin and myoglobin. Subcutaneous fat, near-nerve adipose tissue, and nerve measurements show a clear double dip between 500 and 600 nm, indicating the presence of oxyhemoglobin. The resemblance of nerve and subcutaneous fat in the spectral range of 400 to 650 nm is in accordance with the comparable levels of hemoglobin/myoglobin and beta-carotene in Figure 3. After 600 nm, the signal generally increases due to the so called "optical window": a wavelength region in which optical absorption in most tissue is relatively low. The near infrared part of the spectrum is dominated by optical absorption of water and fat. Water shows a characteristic local reduction in optical absorption at 1000 to 1160 nm, recognized as an intensity peak in the spectra measured on muscle and nerve indicated by a gray ellipse in Figure 2. A characteristicly sharp intensity dip around 1200 nm due to high lipid concentration is appreciable in the spectra measured on subcutaneous fat and near-nerve tissue. The difference between near-nerve and on-nerve tissue is far more distinct in the infrared part of the spectrum, a wavelength region invisible for the human eye. Examples of these differences are the sharp dip at ~1200 nm and the increase in intensity after 1450 nm in the near-nerve spectrum compared to the on-nerve spectrum. In the fluorescence spectra, the difference in area under the curve between the tissue groups is most notable. Muscle measured a remarkably low fluorescence signal. Fluorescence intensity is influenced by the presence of fluorescent molecules as well as the absorption of the excitation/emission photons; the low fluorescence signal in muscle may be explained by strong optical absorption of the excitation or emission photons due to the large amount of myoglobin. Furthermore, the typical absorption of hemoglobin between 500 to 650 nm is also noticeable in the fluorescence spectra of the other tissue types.

Tissue Parameter Quantification

Clinically comprehensive parameters, derived from the measured spectra are visualized in boxplots (Fig. 3). Parameters related to blood: hemoglobin/myoglobin concentration and the oxygen saturation are grouped in the first column. The optical absorbers fat fraction and beta-carotene are shown in the second column. Scattering parameters are grouped in the third column, two parameters derived from the fluorescence spectra (collagen and FS area, the latter being the total fluorescence intensity over the measured wavelengths) form the last column. Adipose tissue (subcutaneous fat and near-nerve) is characterized by high measured lipid and beta-carotene concentrations, but are also high in oxygen saturation and low in hemoglobin. Differences in nerve and muscle ($P < .05$) could be found in oxygen saturation and fluorescence area. When comparing nerve with adipose tissue (subcutaneous fat and near-nerve), significant differences were found in blood content and fat fraction with nerve containing more blood compared to adipose tissue and less fat. Both near-nerve and subcutaneous fat contain significantly more beta-carotene compared to nerve. Although not significant, reasonable amounts of collagen were only found in muscle and nerve.

Tissue Classification

Automated tissue identification using knn classification revealed a MCC of 0.83; positive values (0–1) indicate a positive correlation. Classification showed a sensitivity for nerve identification of 100%, a specificity of 83%, and accuracy 91%. Parameters used in the classification were the amounts of fat and water, fat fraction, hemoglobin, oxygen saturation, Mie scattering and scattering at 800 nm, and total fluorescence intensity. These parameters were

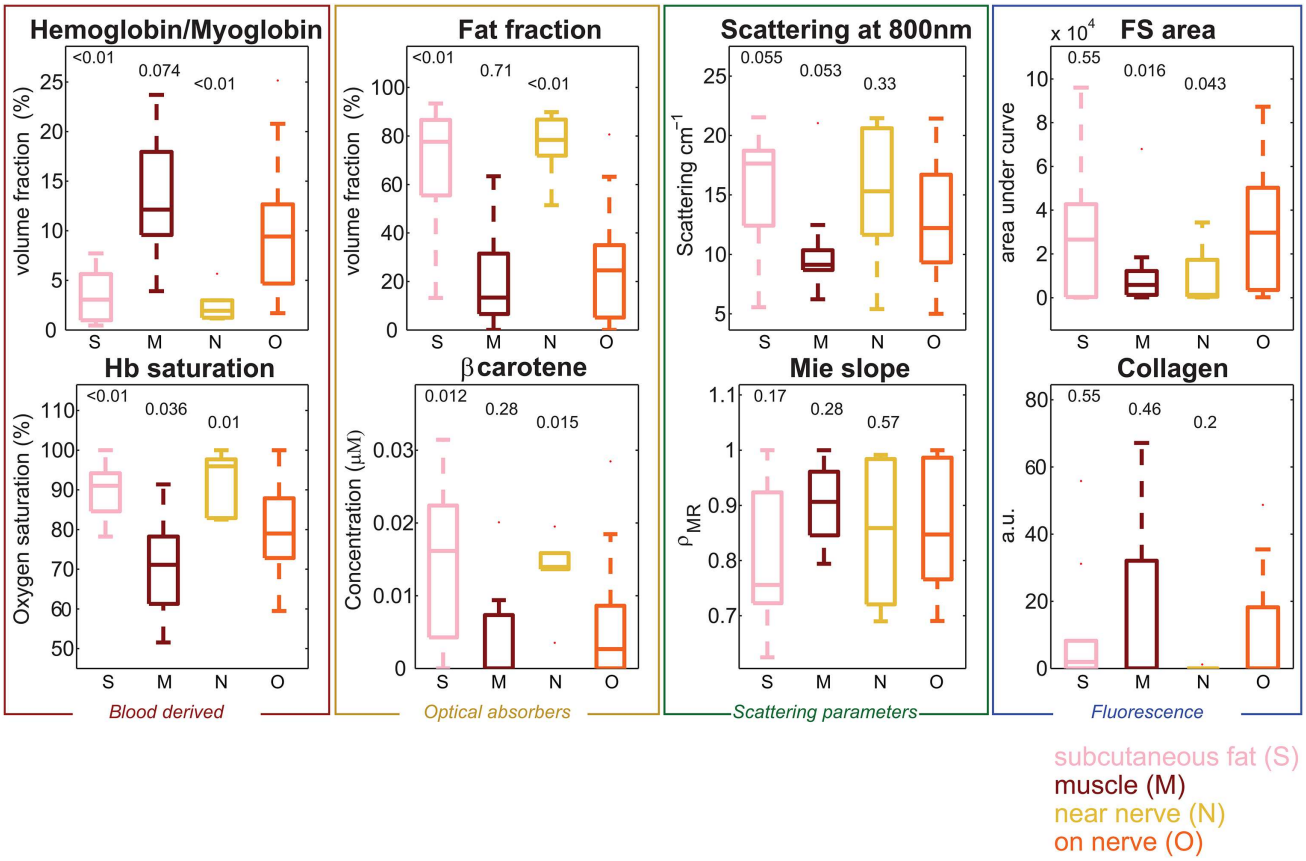

Fig. 3. Boxplots of relevant parameters. Above the bars, the significance levels (p-values) are mentioned for the difference between the average values for the nerve and the specific tissue group, based on a Mann-Whitney-U test.

selected based on the impact on the MCC by systematically excluding specific parameters from the classification.

All parameters selected were derived from the DRS measurements, except fluorescence intensity. Because of measuring time and the technical requirements for fluorescence measurements, it could be beneficial to discard the fluorescence approach. Classification without the fluorescence parameters resulted in a lower MCC of 0.74 with a sensitivity of 88%, specificity of 86%, and an accuracy of 87%. When using PCA on the DRS spectrum only, the 3-knn classification resulted in a MCC of 0.71 with sensitivity 88% and specificity 83%. With the total fluorescence added as extra component, the MCC climbed to 0.78 with a sensitivity of 92% and a specificity of 86%.

DISCUSSION

This human in vivo study shows the potential of DRS/FS to identify nerve branches and to differentiate them from various surrounding tissue based on tissue specific optical properties. Nerve branches could be detected with a sensitivity of 100% and specificity of 83% (accuracy 91%). For a reliable estimation of the potential of the technique, it is important to include all tissue classes in the classification analysis that may cover nerve tissue. Four tissue types were included in this study, subcutaneous fat, muscle, near-nerve adipose tissue and nerve. In some cases, nerves are surrounded by bone. As bone could be identified based on visual appearance and consistency, bone was not included in this study. Tissue specific to a unique anatomical location, like parotid glandular tissue could be evaluated in future research.

Our results are in agreement with other studies that focus on peripheral nerve identification using DRS. Schols et al. targeted the recurrent laryngeal nerve to select spectral features of nerve tissue.[16] In the study, 36 parameters based directly on the measured spectrum (eg, gradients) were selected. The number of measurements was limited to 10 unique locations on-nerve and 5 unique locations on adipose tissue. They reported an accuracy of 67% to 100% depending on the sensor type and classification method.

In a human post-mortem study by Hendriks, the cervical nerves with a circular shaped cross section and a diameter ca. 3 mm were targeted.[30] Multiple classification methods were used to distinguish nerve from surrounding tissue. A MCC ranging from 0.62 to 0.83 was achieved using a Classification and Regression Tree (CART) and Support Vector Machine (SVM) method, respectively. The SVM results showed a sensitivity of 91%, a specificity of 91% and accuracy 91%.

In the present study, physiological fit parameters were used, which translate the measured spectrum into comprehensive clinical parameters. Examples are concentrations of water, fat, beta-carotene and hemoglobin, oxygen saturation, and scattering. An advantage of this approach is that in the clinical setting, the value of each independent

comprehensive parameter can be interpreted by the user, before or after the classification. For example, in a particular clinical context where the amount of blood shows significant variation between measurements, independently from tissue type, the blood parameter can be discarded from the classification algorithm. A potential drawback of our approach is that the information of the spectra that contain hundreds of data points per measurement is reduced to a limited number of parameters, and therefore information may be lost. Clinically comprehensive parameters were used to achieve maximum insight, although this method may not deliver optimal accuracies. Feature reduction using PCA, as an alternative for parameter fitting, was performed to estimate a possible negative effect on the classification outcome. Comparable classification results were obtained from the fit parameter analysis and the PCA analysis (MCC 0.83 vs. 0.78). These results are in line with a comparison between various methods for feature reduction as described earlier.[31] In this study, no prior database of tissue measurements was used; classification was done after collecting the entire dataset. Duration of the classification during this study is not an indication for the intended intra-operative use. Although a tissue classification within seconds is expected, future research should demonstrate the total duration from acquisition to classification.

We observed that with small nerves, the probing volume of the light may include some underlying tissue which could impact the ability to differentiate nerves from surrounding tissues. The nerves measured in this study included the greater auricular nerve, the spinal accessory nerve, and the facial nerve, all measuring 1 to 3 mm and often located in close relation with muscle. Inclusion of some muscle tissue in the probing volume of the nerve measurements explains the similarities in the box plots (Fig. 3) between nerve and muscle tissue which were more distinct in earlier post-mortem nerve and muscle measurements.[30] It should be noted that the measurement volume in DRS is influenced by the distance between the illuminating and the collecting fibers. When the inter-fiber distance is increased light travels a longer path through the tissue. This leads to an increased probed volume as well as an increased penetration depth meaning that for small nerves underlying tissue may be measured as well.[31] For small nerves, like in the present study, the probe volume should be small to prevent such influence from underlying tissues. The penetration depth and therefore the probed volume depends on the optical absorption and scattering of the tissue of interest. As both absorption and scattering vary with the wavelength of the incident light, the penetration depth theoretically depends on the wavelength. This means that optical parameters derived from wavelength regions with high tissue absorption (eg, 400–600 nm and 1200–1700 nm) hold more information about the superficial layers (<2 mm) compared to wavelength regions with less absorption and scattering (eg, 650–1200 nm).

The addition of fluorescence spectroscopy requires an alternative light source, typically a semiconductor laser and an extra set of filters, as well as extra measurement time. Our results show, however, that omitting fluorescence may impact accuracy. Classification accuracy dropped from 91% to 87% when discarding the fluorescence parameter

For this study, we selected nerves that are commonly exposed in head and neck surgery and are at risk of iatrogenic nerve damage. The extensive and careful preparation of the nerves makes this environment preeminently suited for both validation and application of advanced intra-operative nerve identifying techniques. Translation of the results found in open surgery to other applications such as percutaneous nerve identification for anesthetic purposes must be done with caution. Important parameters like oxygen saturation or the presence of blood are probably influenced by tissue preparation during surgery, as may be the exposure to air during the procedure. In this study, optical measurements highly contaminated with blood were excluded. Hemoglobin, and therefore blood, is a strong optical absorber especially in the lower part of the spectrum (400–650 nm). The influence of high amounts of blood could overshadow spectral characteristics of the tissue types. In future research, after identification of distinctive spectral characteristics, the classification method should be tested in various situations. Nevertheless, the influence of hemoglobin on the larger wavelength part of the spectrum (>900 nm) is a lot less significant; spectral characteristics in this part of the spectrum are very likely to resist the influence of contamination by hemoglobin.

The optical technique in the present study was incorporated into a measurement probe, which allows variation in operator use like applied pressure and measurement angle, which may lead to extra variability in the measurements.[32] When incorporated into a surgical tool, variations in angle and pressure could be minimized to improve the robustness of the technique.

Measurements were performed in a controlled environment with measurement locations on carefully identified tissue. Larger clinical studies are necessary to develop a robust algorithm for nerve classification. Furthermore technical development should be initiated to make the technology applicable for routine clinical use. DRS/FS as presented here can be incorporated into smart optical devices with embedded fiber optics allowing real-time identification of tissue during surgery. Examples are presented for regional anesthesia and percutaneous tumor biopsy.[15,33] The exact nature of such a device for surgical guidance needs, however, further consideration.

CONCLUSION

In this in vivo pilot study, small peripheral nerves and surrounding tissue were identified, based on clinically comprehensive parameters derived from the measured spectra. This study clearly shows the potential of DRS/FS for tissue identification with regard to peripheral nerves.

BIBLIOGRAPHY

1. Stelzle F, Zam A, Adler W, et al. Optical nerve detection by diffuse reflectance spectroscopy for feedback controlled oral and maxillofacial laser surgery. *J Transl Med* 2011;9(1):20.

2. Whitney MA, Crisp JL, Nguyen LT, et al. Fluorescent peptides highlight peripheral nerves during surgery in mice. *Nat Biotechnol* 2011;29(4): 352–356.
3. Lewis SR, Price A, Walker KJ, McGrattan K, Smith AF. Ultrasound guidance for upper and lower limb blocks. *Cochrane Database Syst Rev* 2015;9: CD006459.
4. Brown JQ, Bydlon TM, Richards LM, et al. Optical assesssment of tumor resection margins in the breast. *IEEE J Sel Top Quantum Electron* 2010; 16(3):530–544.
5. de Boer L, Molenkamp B, Bydlon T, et al. Fat/water ratios measured with diffuse reflectance spectroscopy to detect breast tumor boundaries. *Breast Cancer Res Treat* 2015;152(3):509–518.
6. Nachabé R, Evers DJ, Hendriks BH, et al. Diagnosis of breast cancer using diffuse optical spectroscopy from 500 to 1600 nm: comparison of classification methods. *J Biomed Opt* 2011;16(8):087010–087012.
7. Evers D, Nachabe R, Hompes D, et al. Optical sensing for tumor detection in the liver. *Eur J Surg Oncol* 2013;39(1):68–75.
8. Tanis E, Spliethoff J, Evers D, et al. Real-time in vivo assessment of radiofrequency ablation of human colorectal liver metastases using diffuse reflectance spectroscopy. *Eur J Surg Oncol* 2016;42(2):251–259.
9. Langhout GC, Spliethoff JW, Schmitz SJ, et al. Differentiation of healthy and malignant tissue in colon cancer patients using optical spectroscopy: A tool for image-guided surgery. *Laser Surg Med* 2015;47(7): 559–565.
10. Schols RM, Dunias P, Wieringa FP, Stassen LP. Multispectral characterization of tissues encountered during laparoscopic colorectal surgery. *Med Eng Phys* 2013;35(7):1044–1050.
11. Chang VT-C, Bean SM, Cartwright PS, Ramanujam N. Visible light optical spectroscopy is sensitive to neovascularization in the dysplastic cervix. *J Biomed Opt* 2010;15(5):057006.
12. Bard MP, Amelink A, Skurichina M, et al. Optical spectroscopy for the classification of malignant lesions of the bronchial tree. *Chest* 2006;129(4): 995–1001.
13. Evers DJ, Nachabé R, Klomp HM, et al. Diffuse reflectance spectroscopy: a new guidance tool for improvement of biopsy procedures in lung malignancies. *Clin Lung Cancer* 2012;13(6):424–431.
14. Brynolf M, Sommer M, Desjardins AE, et al. Optical detection of the brachial plexus for peripheral nerve blocks: An in vivo swine study. *Reg Anesth Pain Med* 2011;36(4):350–357.
15. Balthasar A, Desjardins AE, van der Voort M, et al. Optical detection of peripheral nerves: an in vivo human study. *Region Anesth Pain Med* 2012;37(3):277–282.
16. Schols RM, ter Laan M, Stassen LP, et al. Differentiation between nerve and adipose tissue using wide-band (350–1,830 nm) in vivo diffuse reflectance spectroscopy. *Lasers Surg Med* 2014;46(7):538–545.
17. Hendriks BH, Balthasar AJ, Lucassen GW, et al. Nerve detection with optical spectroscopy for regional anesthesia procedures. *J Transl Med* 2015; 13(1):380.
18. Nachabé R, Sterenborg HJ, Hendriks BH, Desjardins AE, van der Voort M, van der Mark MB. Estimation of lipid and water concentrations in scattering media with diffuse optical spectroscopy from 900 to 1600 nm. *J Biomed Opt* 2010;15(3):037015.
19. Farrell TJ, Patterson MS, Wilson B. A diffusion theory model of spatially resolved, steady-state diffuse reflectance for the noninvasive determination of tissue optical properties in vivo. *Med Phys* 1992;19:879.
20. Doornbos R, Lang R, Aalders M, Cross F, Sterenborg H. The determination of in vivo human tissue optical properties and absolute chromophore concentrations using spatially resolved steady-state diffuse reflectance spectroscopy. *Phys Med Biol* 1999;44(4):967.
21. Spliethoff JW, Evers DJ, Jaspers JE, Hendriks BH, Rottenberg S, Ruers TJ. Monitoring of tumor response to Cisplatin using optical spectroscopy. *Transl Oncol* 2014;7(2):230–239.
22. Zonios G, Dimou A. Light scattering spectroscopy of human skin in vivo. *Opt Express* 2009;17(3):1256–1267.
23. Nachabé R, Hendriks BH, van der Voort M, Desjardins AE, Sterenborg HJ. Estimation of biological chromophores using diffuse optical spectroscopy: benefit of extending the UV-VIS wavelength range to include 1000 to 1600 nm. *Biomed Opt Express* 2010;1(5):1432–1442.
24. Nachabé R, Hendriks BH, Desjardins AE, van der Voort M, van der Mark MB, Sterenborg HJ. Estimation of lipid and water concentrations in scattering media with diffuse optical spectroscopy from 900 to 1600 nm. *J Biomed Opt* 2010;15(3):037015.
25. Spliethoff JW, Evers DJ, Klomp HM, et al. Improved identification of peripheral lung tumors by using diffuse reflectance and fluorescence spectroscopy. *Lung Cancer* 2013;80(2):165–171.
26. de Boer LL, Hendriks BH, van Duijnhoven F, et al. Using DRS during breast conserving surgery: identifying robust optical parameters and influence of inter-patient variation. *Biomed Opt Express* 2016;7(12):5188–5200.
27. Müller M, Hendriks BH. Recovering intrinsic fluorescence by Monte Carlo modeling. *J Biomed Opt* 2013;18(2):027009–027009.
28. Müller MG, Georgakoudi I, Zhang Q, Wu J, Feld MS. Intrinsic fluorescence spectroscopy in turbid media: disentangling effects of scattering and absorption. *Appl Opt* 2001;40(25):4633–4646.
29. Powers DM. Evaluation: from precision, recall and F-measure to ROC, informedness, markedness and correlation. *J Mach Learn Tech* 2011;2(1): 37–63.
30. Hendriks BH, Balthasar AJ, Lucassen GW, et al. Nerve detection with optical spectroscopy for regional anesthesia procedures. *J Transl Med* 2015; 13(1):380.
31. Arifler D, MacAulay C, Follen M, Richards-Kortum R. Spatially resolved reflectance spectroscopy for diagnosis of cervical precancer: Monte Carlo modeling and comparison to clinical measurements. *J Biomed Opt* 2006; 11(6):064027.
32. Chang VT-C, Merisier D, Yu B, Walmer DK, Ramanujam N. Towards a field-compatible optical spectroscopic device for cervical cancer screening in resource-limited settings: effects of calibration and pressure. *Opt Express* 2011;19(19):17908–17924.
33. Spliethoff JW, Prevoo W, Meier MA, et al. Real-time in vivo tissue characterization with diffuse reflectance spectroscopy during transthoracic lung biopsy: a clinical feasibility study. *Clin Cancer Res* 2016;22(2):357–365.